

Coherent Noise Removal in Dark pixels (Case Study: Images Acquired By Landsat 5 Thematic Mapper)

Erfan Amraei¹, Mohammad Reza Mobasheri²

¹Electrical Engineering Department, Khavaran Institute of Higher Education
Mashhad, Iran

²Remote Sensing Department, KNToosi University of Technology
Tehran, Iran

Abstract

Thematic mapper sensor mounted on Landsat 5 satellite is a multispectral sensor with high spatial and spectral resolution. In the images acquired by this sensor from low-reflectance areas, due to high spatial and spectral resolution, signal-to-noise ratio decreases and leads to reduced data quality. A kind of noise is observed in the images acquired by thematic mapper sensor from dark surfaces, such as water surfaces, which is known as coherent noise. On the other hand, one of the most widely used existing methods for atmospheric corrections is using dark pixels. Coherent noise in dark pixels causes errors in atmospheric corrections and image data interpretation. Thus, removing this kind of noise from the images seems necessary. In this paper, image filtering using frequency domain rectangular notch filters has been employed to remove coherent noise from the images acquired by thematic mapper. Reducing standard deviation in the filtered image and increasing PSNR revealed image improvement compared to other methods. To prove the validity of the results, simulated data were used. Subsequently, comparing the filtered image with the original image and also low relative error rate showed the accuracy of proposed method in noise removal.

Keywords: *Thematic Mapper, Coherent Noise, Atmospheric correction, Dark Pixels, Remote Sensing.*

1. Introduction

Thematic mapper sensor, abbreviated as TM, is a multispectral sensor mounted on Landsat 4 and 5. Imaging technique in this sensor is as whisk broom [6]. Thematic Mapper is a sensor with high spectral and spatial resolution. This feature of TM leads to the reduced signal-to-noise ratio. This ratio is particularly very low in images acquired from dark scenes such as water surfaces and subsequently leads to reduced data quality. On the other hand, one of the most widely used atmospheric corrections methods is using dark pixels. In this method, the acquired values in pixels where very low reflectance is expected are identified as atmospheric effects and are used for atmospheric corrections throughout the image. A kind of

noise is observed in images acquired by TM sensor from low-reflectance surfaces which is known as coherent noise (CN). This kind of noise causes errors in atmospheric corrections using dark pixels. Coherent noise appears as a periodic pattern in satellite images [9]. Currently, removing coherent noise for level 1T images of Landsat 5 TM has not been performed [9]. CN influences all detectors used in reflective bands [2]. This noise includes coherent bands in north and north east – south and south west with irregular phase change between two groups of lines [1]. Period of this pattern is about 10-11 pixels and its amplitude is 1-2 digital counts [1]. Unfortunately, not much work has done on removal of coherent noise. To remove CN from Landsat images, [1] has used a series of median filters in spatial domain which are applied to the image iteratively. fast noise removal process and simplicity are among the advantages of this method. The most remarkable defect of this method is that although we can remove CN using this method, this removal may be followed by disturbing the information contained in the images. [3] has explained a kind of similar yet somehow different noise for Multi Spectral Scanner (MSS) and has used frequency domain filters to remove it. This kind of noise is called Nyquist noise [9]. [7] and [8] have used spatial domain image filtering to remove coherent noise from TM sensor images. This method is a simple one for removing the noise, but some residual noise remains in the image after filtering and it is not removed completely. In this paper, frequency domain image filtering using rectangular notch filter has been proposed to remove coherent noise from acquired images by landsat 5 TM sensor. It should be noted that after removing CN in images acquired in band 1, some periodic striping patterns remain for whose removal spatial moment matching method has been used.

2. Material and Methods

2.1 Used Data

Coherent noise in the images acquired in bands 1, 5 and 7 of TM sensor is more prominent. Fig. 1 shows 21 km * 17 km images acquired in these bands from Caspian Sea in August 7, 2010 and 26 July, 2000 which have been pre-processed in level 1T. TM sensor data pre-processing in

level 1T for the images with normal-reflectance surfaces is successful to a large extent, but this method of pre-processing is affected by non-linear behavior of detectors in low-reflectance surfaces and enhancement is unsuccessful for such images [10]. Thus, there are still some noises in pre-processed images in level 1T. To better see the noise in the images, some parts of the images have been enlarged in Fig. 1.

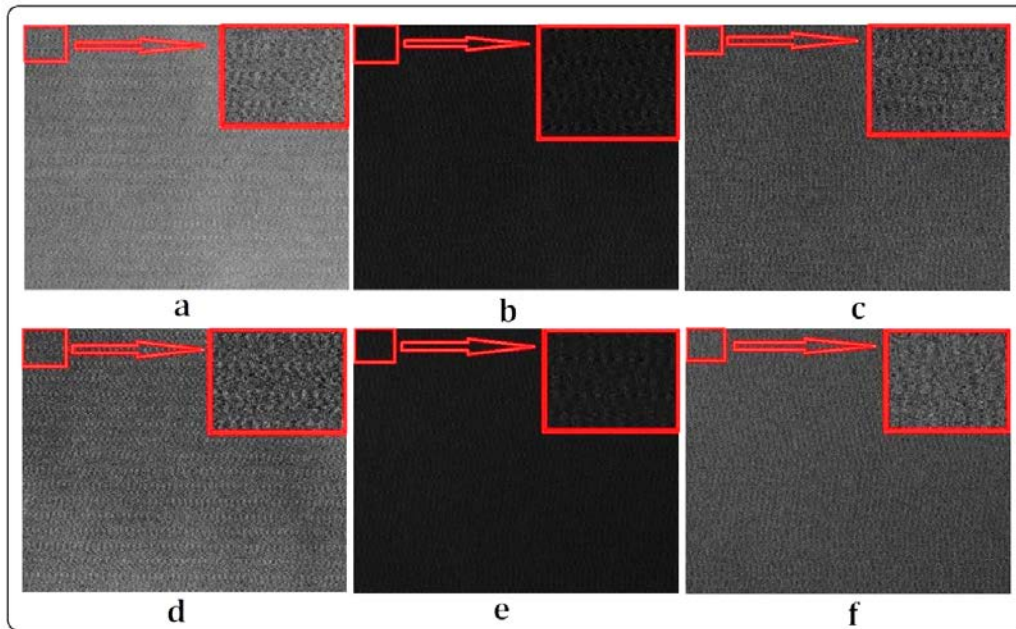


Fig. 1. Images acquired in bands 1, 5 and 7 of Landsat 5 TM from Caspian Sea in 2000 are shown in a, b and c respectively. Also, the images acquired in bands 1, 5 and 7 from Caspian Sea in 2010 are shown in d, e and f respectively.

The diagram in Fig. 2 shows the water reflectance rate in these bands. As seen in this diagram, reflectance rate in these bands is very low and the images acquired from surfaces covered by water are dark.

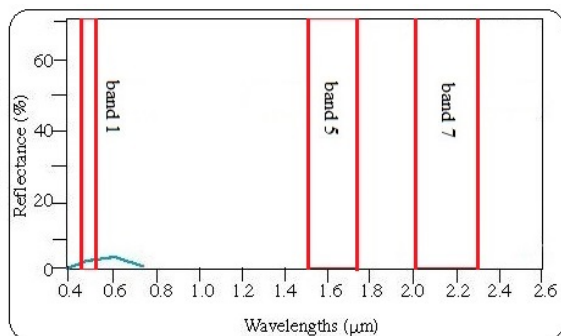


Fig. 2. Spectral diagram of water reflectance. It should be noted that determined range for spectral bands of TM sensor is as full width half maximum (FWHM).

On the other hand, weather condition and wind speed increase can cause breaking the waves and foaming on the water and increase DN in these bands. Therefore, to ensure atmospheric conditions do not have an effect on the carried out studies, information related to atmospheric conditions of the area in mentioned dates were received from Babolsar meteorological station. The information received from this station show the atmospheric stability in the studied area. This information is shown in Table 1. It should be noted that MATLAB R2011a and Bilko 3.3 (Beta) have been used to perform calculations and data corrections.

Table 1. Atmospheric conditions of the studied area

Date of imaging	August 7, 2010	July 26, 2000
Temperature (°C)	24	22
Pressure (hpa)	1015.30	1016.10
Wind speed (m/s)	0	1
Wind direction	-	south

2.2. Noise Removal Method

Equation 1 shows the detector output signal where $X_{(i,j)}$ is the i th detector output signal in i th band, $R_{(i,j)}$ is the signal reached from the scene to the i th detector in i th band and $N_{(i,j)}$ is the noise of the i th detector in i th band.

$$X_{(i,j)} = R_{(i,j)} + N_{(i,j)} \quad (1)$$

By definition, coherent noise includes the combination of similar sinusoidal noises with a constant phase difference. So, N is a sinusoidal noise. The idea in this study is using Fourier transform and transmitting the image to frequency domain, as the result of Fourier transform of sinusoidal functions is complex and conjugate impulses in frequency domain (Equation 2).

$$F\{\sin(an)\} = -i\pi \sum_{k=-\infty}^{\infty} [\delta_{(\omega-a-2k\pi)} - \delta_{(\omega+a+2k\pi)}] \quad (2)$$

To detect coherent noise after transmitting the image to frequency domain, fourier spectrum of the image is calculated and plotted. If fourier transform of the image is according to the relation 3, then relation 4 is used to calculate fourier spectrum.

$$F_{(\omega)} = R_{(\omega)} + iI_{(\omega)} \quad (3)$$

$$|F_{(\omega)}| = [|R_{(\omega)}|^2 + |I_{(\omega)}|^2]^{1/2} \quad (4)$$

In this relation, $R_{(\omega)}$ is the real part and $I_{(\omega)}$ is the imaginary part of the fourier transform. impulses resulting from coherent noise are seen as some bright spots in fourier spectrum. After detecting noise components, frequency domain rectangular notch filter is used to remove them. A notch filter removes the certain frequencies located in the center of the notch. From the most prominent advantages of these filters is having sharp

edges and low ripple [4]. It should be noted that after removing the coherent noise in the images in band 1, some minor periodic striping patterns remain in the image for whose removal spatial moment matching method is used. In this method, statistical moments, such as mean and standard deviation of detectors in each band, are used to balance statistical characteristics of the detector arrays to those reference values [5]. Let m_{ik} i th detector mean in k th band and σ_{ik} standard deviation of i th detector in k th band. In addition, \bar{m}_{ik} and $\bar{\sigma}_{ik}$ are reference values for these moments. After calculating these moments, gain coefficient α_{ik} and offset β_{ik} should be calculated for each detector. Image data for i th sample, i th row and k th band (x_{ijk}) are modified using relation 5:

$$x'_{ijk} = \alpha_{ik} x_{ijk} + \beta_{ik} \quad (5)$$

Gain and offset are calculated by the following relations:

$$\alpha_{ik} = \frac{\bar{\sigma}_{ik}}{\sigma_{ik}} \quad (6)$$

$$\beta_{ik} = \bar{m}_{ik} - \alpha_{ik} m_{ik} \quad (7)$$

In these relations, gain coefficient controls the image columns standard deviation and offset controls the mean [5].

3. Results and Analysis

The method provided in 2.2 was applied to the images shown in Fig. 1. Fig. 2 shows the fourier spectrum of original images. As seen in the figure, noise components are seen as some impulses in frequency domain which have been marked in the figure.

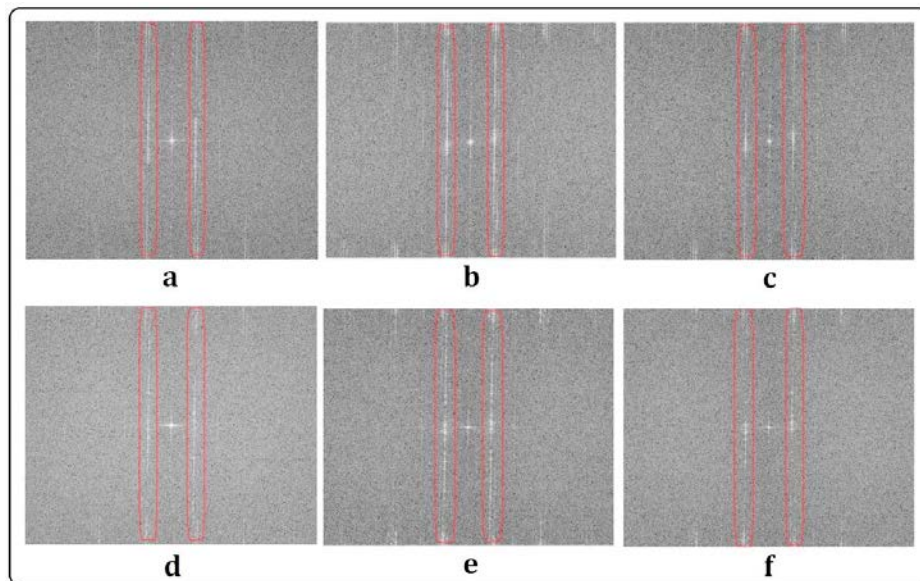


Fig. 2. Fourier spectrum of the raw images shown in Fig. 1. Red frame marks the impulses related to the noise.

Fig. 3 shows the results of noise removal from images in Fig.1. As it is observed, coherent noise in the raw images does not exist any longer in these images which indicate

that noise has been removed. As seen in the figure, some striping patterns are seen in the filtered images of band 1.

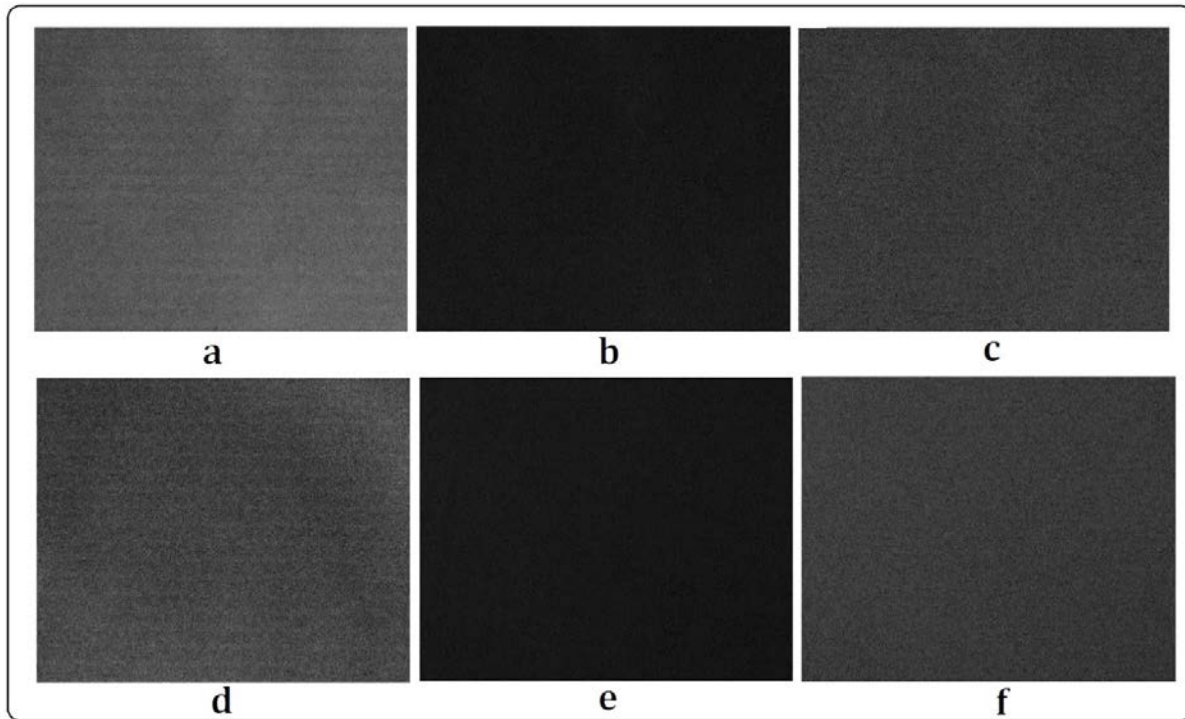


Fig. 3. The results of noise removal from the images shown in Fig.1 (a) to (f) have been shown in Figure (a) to (f) respectively. Some minor striping patterns are seen in the filtered images of band 1.

Also, Fig. 4 shows the results of removing striping patterns from the filtered images of band 1. Visual investigations show the successful removal of striping patterns.

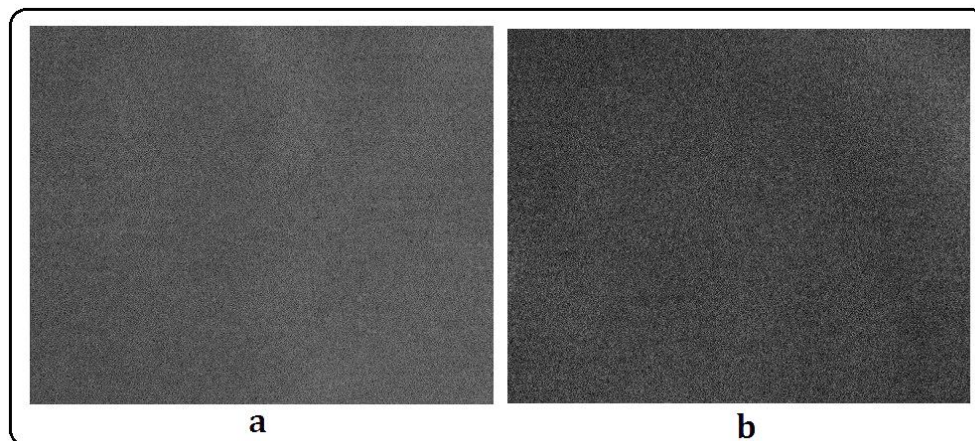


Fig. 4. The results of removing striping noise from images in Fig.3 (a) and (c) have been shown in (a) and (b) respectively.

Fig. 6 shows fourier spectrum related to the images in Fig. 3. As seen in this figure, amplitude of coherent noise

components has been reduced after filtering which indicates noise removal.

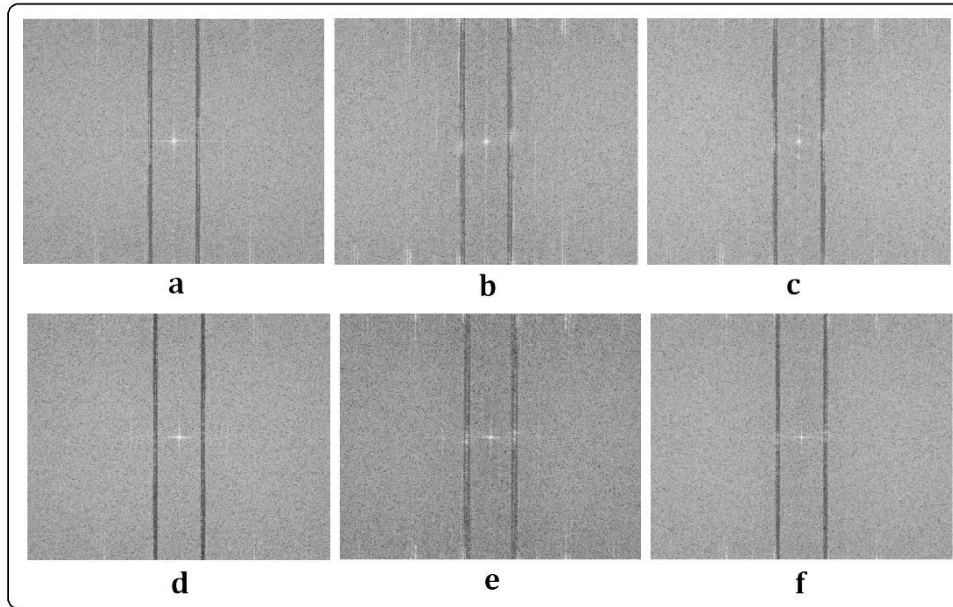


Fig. 6. Fourier spectra of the images in Fig. 3 (a) to (f) have been shown in Figs. (a) to (f) respectively.

To evaluate the effectiveness of the proposed method in noise removal, histogram of the images before and after the filtering were investigated and some statistical parameters such as mean and standard deviation were calculated for these images. histograms of the raw and the filtered images in bands 5 and 7 are shown in Fig. 7. Also,

histograms of the raw and the filtered images (after removing coherent noise and striping noise) in band 1 are shown in Fig. 8. As seen in histograms before and after the filtering, behavior of the histogram has become better and data diversity in images has increased.

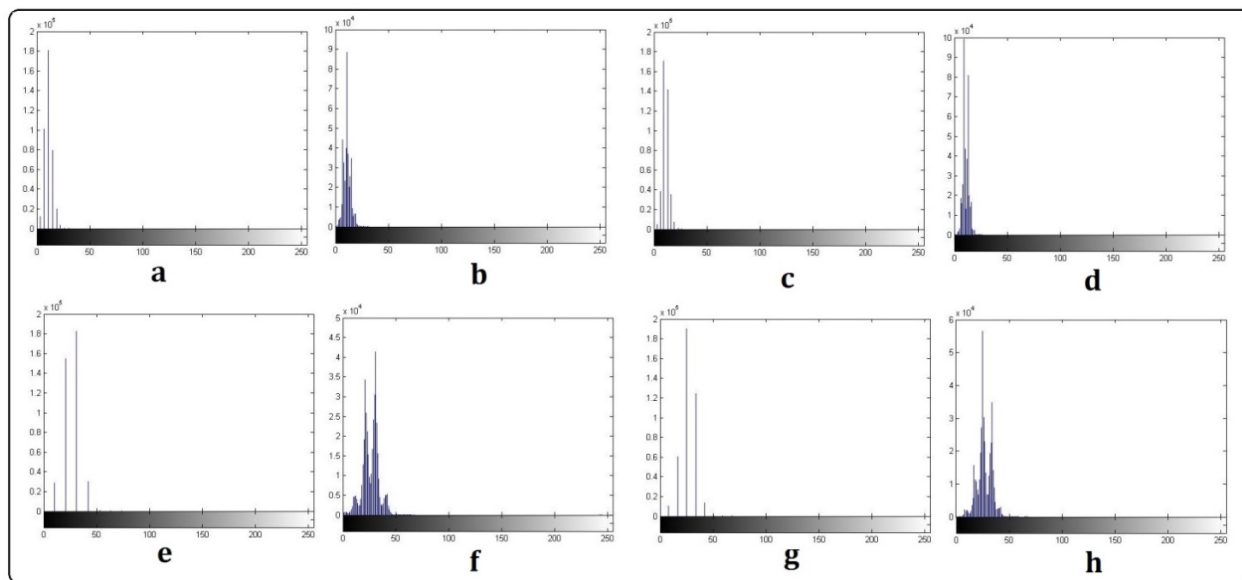


Fig. 7. Histograms in band 5 and 7 before and after the filtering. (a) and (b): histograms of data acquired in 2000 in band 5 before and after the filtering. (c) and (d): histograms of data acquired in 2010 in band 5 before and after the filtering. (e) and (f): histograms of data acquired in 2000 in band 7 before and after the filtering. (g) and (h): histograms of data acquired in 2010 in band 7 before and after the filtering.

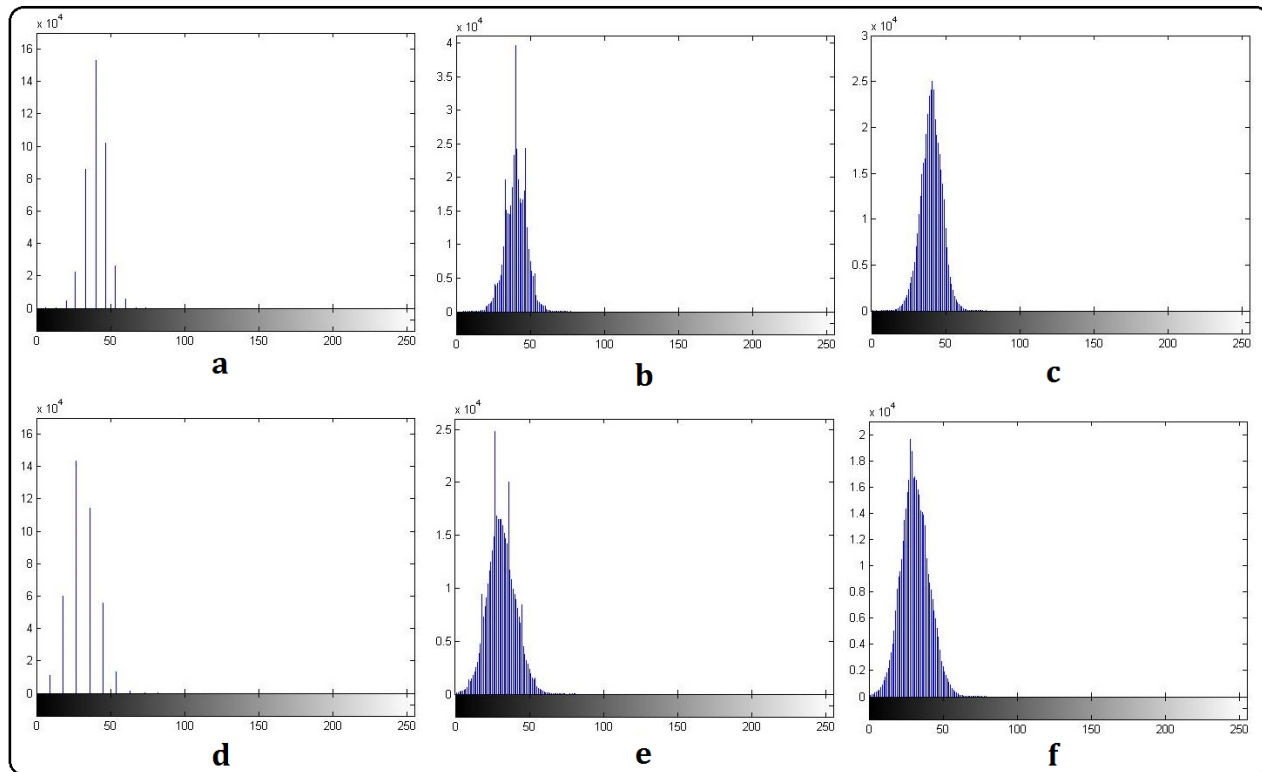


Fig. 8. (a) histograms of the raw image acquired in band 1 in 2000. (b) histograms of the image in band 1 after removal of coherent noise. (c) histograms of the image after removal of striping patterns. (d) histograms of the raw image acquired in band 1 in 2010. (e) histograms of the image in band 1 after removal of coherent noise. (f) histograms of the image after removal of striping patterns.

Tables 2 and 3 show mean and standard deviation before and after noise removal respectively for images in bands 5,

7 and 1. As it is evident, decrease in standard deviation indicates removal of noise from the images.

Table 2. Mean and standard deviation of the images in bands 5 and 7 before and after noise removal.

Date of imaging	Mean (raw image)		SD (raw image)		Mean (filtered image)		SD (filtered image)	
	Band 5	Band 7	Band 5	Band 7	Band 5	Band 7	Band 5	Band 7
August 7, 2010	10.85	26.72	3.24	7.11	10.85	26.72	2.88	6.73
July 26, 2000	10.97	26.22	3.78	8.22	10.97	26.22	3.33	7.72

Table 3. Mean and standard deviation of the images in band 1 before and after coherent noise and striping patterns removal.

Date of imaging	Mean (raw image)	SD (raw image)	Mean (filtered image)		SD (filtered image)	
			After coherent noise removal	After destriping	After coherent noise removal	After destriping
August 7, 2010	40.39	7.54	40.39	40.4	7.05	6.63
July 26, 2000	31.15	10.15	31.15	31.14	9.4	9.02

High value of standard deviation relative to the mean in band 1 and band 7 means that sea surface pixels in the

studied area have had a different interaction with the light which can be attributed to the active substances in the

water. In addition, MSE and PSNR quantities have been calculated to compare the proposed method in this paper with the method proposed in [1]. [1] has used a series of median filters iteratively to remove coherent noise. The relations used for calculating these quantities have been shown in equations 8 and 9.

$$MSE = \frac{1}{M \times N} \sum_{j=0}^{M-1} \sum_{i=0}^{N-1} (g(i,j) - f(i,j))^2 \quad (8)$$

$$PSNR = 10 \log \left(\frac{D^2}{MSE} \right) \quad (9)$$

In these relations, $f(i,j)$ shows the raw image, $g(i,j)$ is the filtered image and (M, N) are image dimensions. It should be noted that D for n -bit quantification equals to 2^n . smaller MSE and larger PSNR show the better performance of the algorithm. The results of calculating these quantities are shown in table 4.

Table 4. The results of calculating MSE and PSNR for both the proposed method in this paper and methods proposed in [1]

Date of imagin g	Band 1				Band 2				Band 3			
	MSE		PSNR (dB)		MSE		PSNR (dB)		MSE		PSNR (dB)	
	Proposed method in [1]	Proposed method in this paper	Proposed method in [1]	Proposed method in this paper	Proposed method in [1]	Proposed method in this paper	Proposed method in [1]	Proposed method in this paper	Proposed method in [1]	Proposed method in this paper	Proposed method in [1]	Proposed method in this paper
August 7, 2010	94.33	16.16	28.38	36.04	10.04	1.98	38.09	45.16	51.87	4.75	30.97	41.36
July 26, 2000	49.77	9.27	31.16	38.45	13.87	2.94	36.7	43.43	73.44	7.17	29.47	39.57

To prove the results obtained from comparison of the proposed method in this study and the method proposed in [1], simulated data for coherent noise have been used. As mentioned before, coherent noise includes a combination of similar sinusoidal functions with a constant phase difference. Sinusoidal functions in frequency domain are seen as some complex and conjugate impulses. Therefore, to add coherent noise to the image, it is transmitted to the frequency domain and then some complex and conjugate impulses are added to fourier transform and then inverse fourier transform is obtained. Fig. 9 (a) and Fig. 9 (b) show

the original and the simulated image for coherent noise respectively. Also, Fig. 9 (c) and Fig. 9 (d) show the images filtered by the proposed method and the method in [1]. Fig. 10 shows the fourier spectrum of the original image and the noisy image (Fig. 9 (a) and (b)). In this figure, the manner in which the noise is added to the original image has been shown. In addition, histograms of the images 9 (a) to (f) have been shown in Fig. 11 (a) to (d).

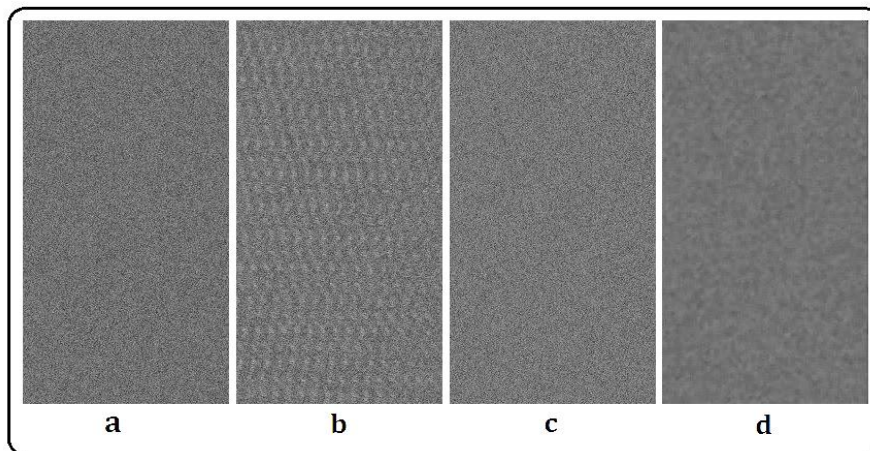


Fig. 9. (a) original image, (b) simulated image for coherent noise, (c) the result of image filtering by the method proposed in this paper, d) the result of image filtering by the proposed method in [1].

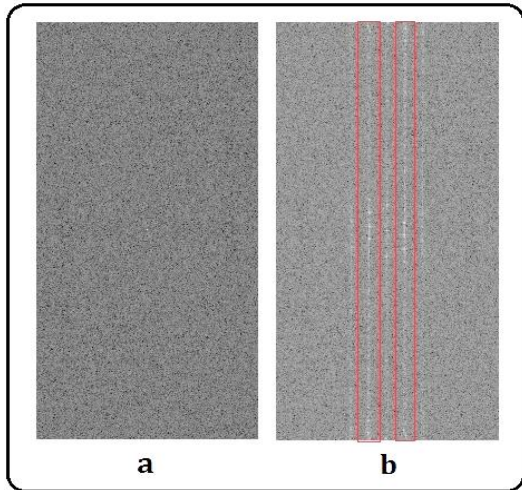


Fig. 10. (a) Fourier spectrum of original image (fig. 9 (a)), (b) Fourier spectrum of simulated image (fig. 9 (b))

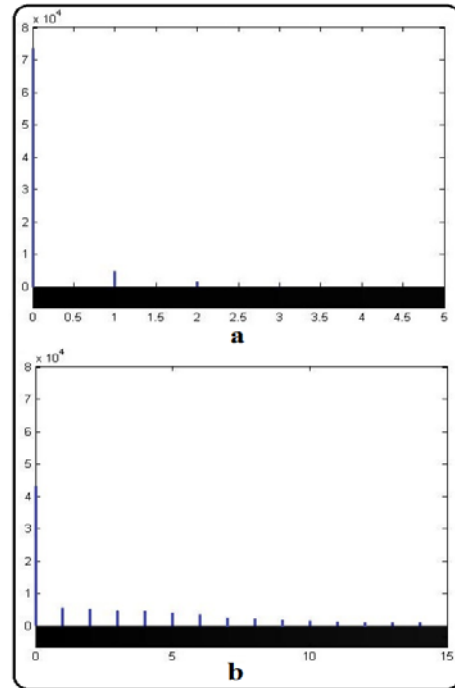


Fig. 12. Histogram of the image resulted from the difference of the images in Fig. 9(a), (c) and (d)

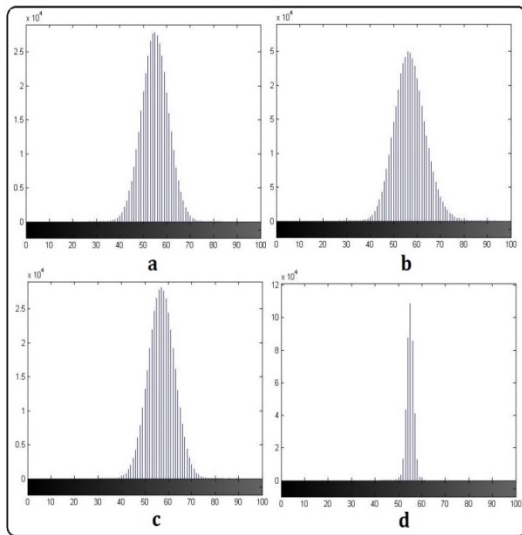


Fig. 11. (a) histogram of Fig. 9 (a); (b) histogram of Fig. 9 (b); (c) histogram of Fig. 9 (c); (d) histogram of Fig. 9 (d)

Fig. 12 (a) and (b) respectively show the histograms of difference images (difference of image in Fig. 9 (a) from the image in Fig. 9 (c) and (d)). In ideal mode, histogram should only show the zero DN. As seen in the histogram of Fig. 12(a), the highest frequency is on zero which consists about 93 percent of total number of image pixels which shows the accuracy of the proposed method in this paper in coherent noise removal. In Fig. 12(b), the highest frequency is also on zero which includes about 50 percent of the pixels in the image. Therefore, removing coherent noise by median filter has a large effect on radiometric information of the image.

To evaluate and compare the results from proposed method in this paper with the results from proposed method in [1], RMSE (Equation 10) has been used. To this aim, RMSE is calculated between corresponding pixels of the filtered image (Fig. 9(c) and (d)) and the original image (Fig. 9 (a)).

$$RMSE = \sqrt{MSE} \quad (10)$$

MSE relation has been shown in the equation 8. Then, RMSE is divided into the filtered image pixels mean to calculate the relative error (Equations 11 and 12).

$$\mu = \frac{\sum_{i=1}^N x_i}{N} \quad (11)$$

$$Relative-error = \frac{RMSE}{\mu} \times 100 \quad (12)$$

Relative error rates for both methods compared to the original image has been shown in Table 5.

Table 5. Calculated values of RMSE and relative error for both methods compared to the image in Fig. 9(a)

	RMSE	μ	Relative error (percent)
Results from the model proposed in this study	0.39	57.03	0.6
Results from the model proposed in [1]	4.02	54.94	7.33

In addition, scatter plot has been plotted between the images of Fig. 9 ((a) and (c)) and also (9 (a) and (d)) (Fig. 13). scatter plot indicates the extent of similarity of two images to each other. Dispersion of points around the first quarter bisection shows the large similarity of the two compared images.

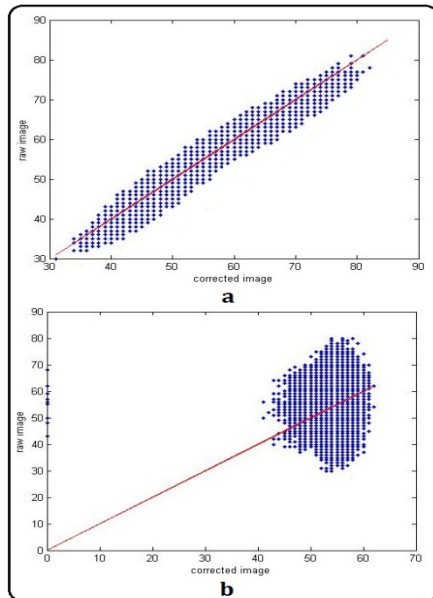


Fig. 13. (a) scatter plot of pixels between Fig. 9(a) and (c). (b) scatter plot of pixels between Fig. 9(a) and (d).

4. Conclusion

Landsat 5 TM is a multispectral sensor which imaging of the earth in 7 bands from visible spectral region to thermal infrared in whisk broom imaging mode. TM is a sensor with high spectral and spatial resolution power. Therefore, in the low-reflectance scene such as water surfaces, signal-to-noise ratio decreases which leads in reduced data quality and appearance of noise in the images. Coherent noise contained in the images acquired from water surfaces by TM sensor is one of such noises. On the other hand, one of the most widely used methods in atmospheric corrections is using dark pixels. In this method, the values received in the low-reflectance pixels are identified as atmospheric effects and are used for atmospheric corrections throughout the image. Thus, coherent noise in dark pixels causes errors during doing atmospheric corrections. In this paper, frequency domain image filtering using notch filters has been proposed to remove coherent noise. After removing coherent noise in images in band 1, some horizontal striping noise still remain in the images for whose removal spatial moment matching method has been used. In this method, statistical moments such as mean and

standard deviation of detectors are used to balance statistical characteristics of the detectors arrays to those reference values. To evaluate the results, noise images and data histograms were analyzed and mean and standard deviation were calculated before and after noise removal. Also, MSE and PSNR were used for comparing the proposed method in this paper with the method in [1]. Results of calculating these quantities showed effectiveness of this method in coherent noise removal. To prove these results, simulated data for coherent noise were used and relative error was calculated for the original image and the filtered image in two presented methods and scatter plots were plotted for them as well.

Reference

- [1] NICHOL. J. E, VOHORA. V, Noise over water surfaces in Landsat TM images, INT. J. REMOTE SENSING, VOL. 25, NO. 11, 2087–2094, 2004.
- [2] Dennis L. Helder, Timothy A. Ruggles, Landsat Thematic Mapper Reflective-Band Radiometric Artifacts, IEEE TRANSACTIONS ON GEOSCIENCE AND REMOTE SENSING, VOL. 42, NO. 12, DECEMBER 2004.
- [3] TILTON, C. J., MARKHAM, B. L., and ALFORD, W. L., Landsat 4 and Landsat 5 MSS coherent noise: characterisation and removal. Photogrammetric Engineering and Remote Sensing, 51, 1263–1279, 1985.
- [4] Gonzalez. R. C, Woods R. E, Eddins S. L, "Digital Image Processing Using MATLAB". Beijing: Publishing House of Electronics Industry, 2009.
- [5] Bisun. D, Tim R. McVicar, Tom G. Van Niel, David L. B. Jupp, Jay S. Pearlman, preprocessing EO-1 Hyperion hyperspectral data to support the application of agricultural indexes, IEEE TRANSACTIONS ON GEOSCIENCE AND REMOTE SENSING, VOL. 41, NO. 6, JUNE 2003.
- [6] Landsat—A Global Land-Imaging Mission, U.S. Department of the interior, U.S. Geological Survey, 2013.
- [7] Zhang, M., Carder, K., Lee, Z., Muller-Karger, F. E., & Goldgof, D. B. Noise reduction and atmospheric correction for coastal applications of Landsat TM imagery. Remote Sensing of the Environment, 70, 167– 180. 1999.
- [8] Thomas, A., Byrne, D., Weatherbee, R., Coastal sea surface temperature variability from Landsat infrared data, Remote Sensing of Environment 81, 262– 272, 2002.
- [9] June.01.2014. [Online]. Available: http://landsat.usgs.gov/science_an_cn.php
- [10] June.01.2014. [Online]. Available: https://landsat.usgs.gov/science_L4-5_Cal_Notices.php